

**Dopamine D1 Receptor Agonist PET Tracer Development: Assessment in Non-Human
Primates**

Olivier Barret^{1,2}, Lei Zhang³, David Alagille^{1,4}, Cristian C. Constantinescu¹, Christine Sandiego¹,
Caroline Papin¹, Jenna M. Sullivan¹, Thomas Morley¹, Vincent M. Carroll¹, John Seibyl¹, Jianqing
Chen⁵, Chewah Lee³, Anabella Villalobos³, David Gray^{3,6}, Timothy J. McCarthy⁵, Gilles
Tamagnan^{1,4}

¹ Invicro, LLC, 60 Temple St., Suite 8B, New Haven, CT, 06510, USA

² Université Paris-Saclay, CEA, CNRS, MIRCen, Laboratoire des Maladies Neurodégénératives,
92265, Fontenay-aux-Roses, France

³ Medicine Design, Medicinal Chemistry, Pfizer Inc., 610 Main Street, Cambridge, MA 02139,
USA

⁴ Xing Imaging, 760 Temple St., New Haven, CT, 06510, USA

⁵ Digital Medicine and Imaging, Early Clinical Development, Pfizer Inc., 610 Main Street,
Cambridge, MA 02139, USA

⁶ Cerevel Therapeutics, 131 Dartmouth St, Boston, MA 02116, USA

Address Correspondence to Dr Olivier Barret, MIRCen, CEA Centre de Fontenay-Aux-Roses, 18
Route du Panorama – BP 6, Fontenay-Aux-Roses Cedex 92265, France

E-mail: olivier.barret@cea.fr

Running title: D1 receptor agonist PET tracer

Keywords: D1 receptor, agonist, PET imaging, schizophrenia, Parkinson's disease

Word counts: 5,127

ABSTRACT

Objective: Non-catechol based high affinity selective dopamine D1 receptor (D1R) agonists were recently described, and candidate PET ligands were selected based on favorable properties. The objective of this study was to characterize *in vivo* in non-human primates two novel D1R agonist PET radiotracers, racemic ^{18}F -MNI-800 and its more active atropisomeric (-)-enantiomer ^{18}F -MNI-968.

Methods: Ten brain PET experiments were conducted with ^{18}F -MNI-800 in two adult rhesus macaques and two adult cynomolgus macaques, and eight brain PET experiments were conducted with ^{18}F -MNI-968 in two adult rhesus macaques and two adult cynomolgus macaques. PET data were analyzed with both plasma-input and reference-region based methods. Whole-body PET images were acquired with ^{18}F -MNI-800 for radiation dosimetry estimates in two adult rhesus macaques.

Results: ^{18}F -MNI-800 and ^{18}F -MNI-968 exhibited regional uptake consistent with D1 receptor distribution. Specificity and selectivity were demonstrated by dose-dependent blocking with the D1 antagonist SCH-23390. ^{18}F -MNI-968 showed a 30% higher specific signal compared to ^{18}F -MNI-800, with a binding potential BP_{ND} of ~ 0.3 in the cortex and ~ 1.1 in the striatum. Dosimetry radiation exposure was favorable, with an effective dose of ~ 0.023 mSv/MBq.

Conclusion: ^{18}F -MNI-968 (^{18}F -PF-0110) has significant potential as a D1R agonist PET radiotracer, and further characterization in human subjects is warranted.

INTRODUCTION

Dopamine D1 receptors (D1R) are the most abundant dopamine receptor subtype in the brain and the primary subtype in the prefrontal cortex (1,2), and are exclusively found post-synaptically on dopamine receptive neurons (medium spiny neurons in the striatum and pyramidal neurons in prefrontal cortex). Despite its extensive brain distribution, D1R interest has dropped behind other subtypes, especially D2 receptors, due in part to the lack of D1R-selective agents that would facilitate a greater understanding of this target.

Dihydroxidine, the first high affinity catechol based selective full D1R agonist, demonstrated the therapeutic potential of D1R-selective ligands in schizophrenia (alleviation of cognitive deficit and negative symptoms (3)) and Parkinson's disease (anti-parkinsonian action in MPTP-treated primate model (4)). The recent introduction of non-catechol based high affinity selective D1R agonists has revived interest in this target (5-9).

The development of *in vivo* imaging techniques has proven extremely valuable to elucidate disease pathology and progression, and advancement of target specific therapies. Several PET radiotracers for D1R have been developed, mainly the antagonists ¹¹C-NNC-112 (10), ¹¹C-SCH-23390 (11), ¹¹C-A-69024 (12), the partial agonist ¹¹C-N-methyl-NNC 01-0259 (13), and the agonist ¹¹C-SKF 82957 (14). However, ¹¹C-SCH-23390 and ¹¹C-NNC-112 suffer from selectivity against 5-HT_{2a} (15), and ¹¹C-N-methyl-NNC 01-0259 and ¹¹C-SKF 82957 have brain-penetrating radio-metabolites (13,14). Moreover, D1Rs exhibit both high and low affinity states, where agonists preferentially bind to the high affinity active state while antagonists do not discriminate between the two states. Therefore, development of a full D1R agonist PET tracer could provide important *in vivo* functional information and be a useful imaging tool to assess D1R agonists.

Two novel D1R agonists from a non-catechol chemotype discovered by Pfizer were selected based on favorable properties as potential PET ligands. The objective of this study was to characterize these two D1R agonist PET radiotracers, racemic ^{18}F -MNI-800 (^{18}F -PF-8477) and the atropisomeric (-)-enantiomer ^{18}F -MNI-968 (^{18}F -PF-0110), *in vivo* in non-human primates (NHP). We assessed their brain distribution and kinetic profile, specificity of the signal in pre-blocking studies with a D1R antagonist and partial agonist, test-retest variability assessment, and estimation of radiation dosimetry of ^{18}F -MNI-800 (^{18}F -PF-8477).

MATERIALS AND METHODS

In Vitro Pharmacology and PET Properties of Novel Non-Catechol D1R Agonists

The identification of a suitable PET ligand was guided by a set of PET properties to find a D1R selective agonist that resides within favorable physicochemical property space defined by CNS PET multiparameter optimization (MPO) score (>3) (16), and shows potent binding affinity to D1R receptor ($B_{\text{max}}/K_d > 10$), high passive permeability (RRCK $P_{\text{app AB}} > 5 \times 10^{-6}$ cm/s), low p-glycoprotein (Pgp) efflux (MDR1 BA/AB ≤ 2.5), and sufficient fraction unbound in brain ($cF_{u_b} > 0.05$) for low non-specific binding.

Initially, racemate PF-8477 (MNI-800) and subsequently its (-)-enantiomer PF-0110 (MNI-968), a non-catechol D1R agonist from a chemotype developed by Pfizer (7), emerged as a promising PET ligand lead with a benzyl fluoride moiety for late-stage fluorine-18 radiolabeling (Figure 1, Supplemental Scheme 1).

Indeed, PF-0110 (MNI-968) has a potent binding affinity to human D1R receptor ($K_i = 2$ nM), and minimal species differences in rat ($K_i = 8$ nM) and NHP ($K_i = 2$ nM). Given a D1R B_{max} in human and NHP striatum of ~ 52 pmol/g tissue (~ 52 nM assuming 100 mg protein/g tissue) (17),

a desired $B_{\max}/K_d > 10$ corresponds to a binding affinity < 5 nM, indicating that PF-0110 (MNI-968) meets this affinity requirement. Moreover, unlike other known D1R antagonist radiotracers (SCH-23390 and NNC-112), PF-0110 (MNI-968) is a potent D1R functional agonist with an EC_{50} of 5 nM and 96% E_{\max} . Finally, PF-0110 (MNI-968) showed selectivity for D1R over other dopamine receptors with no appreciable binding to human D2, D3 and D4 receptors ($IC_{50} > 10$ μ M).

In addition to its favorable in vitro pharmacology profile, PF-0110 (MNI-968) met all the PET ligand property parameters: high CNS PET MPO score (3.57), good passive permeability (RRCK P_{app} AB = 21.6×10^{-6} cm/s), low Pgp efflux (MDR1 BA/AB = 1.46), and reasonable fraction unbound in brain ($cF_{u_b} = 0.06$) suggesting low risk of non-specific binding.

Details on the synthesis of PF-0110 (MNI-968) and PF-8477 (MNI-800) are provided in the supplementary materials.

Radiochemistry of ^{18}F -MNI-800 (^{18}F -PF-8477) and ^{18}F -MNI-968 (^{18}F -PF-0110)

All ^{18}F -MNI-800 and ^{18}F -MNI-968 radiolabeling reactions were performed using a GE TRACERlab FX-FN automated synthesis module using the Boc-protected benzyl chloride precursor (Figure 2, MNI-799 or MNI-969).

For ^{18}F -MNI-800, the two-step, one-pot production with the racemic precursor MNI-799 afforded sufficiently high yields (15-35%) with high radiochemical purity ($> 95\%$), chemical purity (< 0.20 $\mu\text{g/mL}$) and specific activity (> 220 GBq/ μmol).

For ^{18}F -MNI-968, it proved too difficult to confidently control the undesired racemization of the enantiopure precursor MNI-969, and the procedure was modified. First, an in-process chiral high-performance liquid chromatography (HPLC) separation step with inclusion of a chiral

column before the C18 reverse phase column provided sequential separation of the desired atropisomer followed by mass purification. Second, the radiolabeling solvent was changed to acetonitrile as DMSO was not compatible with the chiral stationary phase. Beyond these two changes, ^{18}F -MNI-968 process was similar to ^{18}F -MNI-800 and provided the desired product in expected lower yields (5-15%) and acceptable chemical profile (radiochemical purity > 95%, chemical purity < 0.10 $\mu\text{g}/\text{mL}$, and specific activity > 75 $\text{GBq}/\mu\text{mol}$). Atropisomeric purity was assessed to confirm enantiopurities > 99% at the end of synthesis, throughout storage in solution, and prior to injection.

Details on the radiosynthesis of ^{18}F -MNI-800 and ^{18}F -MNI-968 are provided in the supplementary materials.

Animals

All experiments were conducted in accordance with the United States Public Health Service's Policy on Humane Care and Use of Laboratory Animals and with institutional approval (Yale PET Center, New Haven, CT and Charles River Laboratories, Mattawan, MI). Adult rhesus macaques (*Macaca mulatta*, 2 females (7.6 ± 1.4 kg, NHP A and B) and 1 male (19.6 ± 3.0 kg, NHP C)) and cynomolgus macaques (*Macaca fascicularis*, 3 males, 5.0 ± 0.4 kg, NHP D-F) were studied. Animals were anesthetized with intramuscular ketamine and given glycopyrrolate to reduce secretions, transferred to the camera, and intubated for continuous anesthesia with ~2.5% isoflurane. Radiotracer was injected 2 hours after administration of anesthetics to allow for stabilization of the animals' physiology. Body temperature was maintained by a heated water blanket and monitored with a rectal thermometer.

Blocking Agent Preparation and Administration

SCH-23390 (Sigma-Aldrich, R(+)-SCH-23390 hydrochloride) and PF-2562 (8,9) are potent, selective D1R antagonist and partial agonist, respectively. SCH-23390 was dissolved in normal saline. PF-2562 was dissolved in 5% ethanol, 5% cremophor and 18.5% sulfobutylether- β -cyclodextrin in sterile water.

Receptor occupancy experiments were performed with ^{18}F -MNI-800 and 4 doses of SCH-23390 (0.03, 0.1, 0.2 and 0.5 mg/kg) administered intravenously over a 20-min period beginning 25 min before the radiotracer injection, and with ^{18}F -MNI-968 and 1 dose of PF-2562 in duplicate (1.2 mg/kg total dose) administered intravenously over a 120-min period beginning 30 min before tracer injection (bolus of 0.121 mg/kg/min for 3 min followed by infusion of 0.007 mg/kg/min for 117 min). Plasma samples were taken at several time-points during each PET scan.

Brain PET Studies

PET scans were performed on a Siemens Focus 220 microPET camera (Siemens Healthcare Molecular Imaging, Knoxville, TN, USA) after intravenous bolus administration of ^{18}F -MNI-800 (170.5 ± 16.5 MBq, 0.28 ± 0.22 μg) or ^{18}F -MNI-968 (158.0 ± 29.1 MBq, 0.47 ± 0.22 μg). Ten scans were done with ^{18}F -MNI-800, and eight scans were done with ^{18}F -MNI-968 (see Table 1 for details). Test and retest scans were separated by 2 weeks for ^{18}F -MNI-800 and 4 months for ^{18}F -MNI-968. The dynamic series were reconstructed using filtered back projection with corrections for random, scatter, and attenuation.

Arterial Input Function. After tracer administration, radial artery blood samples were collected over 2 hours. Radioactivity in whole blood and plasma was measured in all samples.

Radio-metabolites were measured in a subset of samples by reverse-phase HPLC performed on a Phenomenex Luna C18(2) (10 x 250 mm, 10 μ m) at a flow rate of 4 mL/min. The mobile phase consisted of a mixture of methanol / water with 0.2% of triethylamine in a 65/35 ratio. Plasma samples were processed by acetonitrile denaturation, and plasma protein binding free fraction (f_p) was measured by ultrafiltration (Centrifree®, Millipore).

Image Processing. PET images were analyzed in PMOD 3.609 (PMOD Technologies, Zurich, Switzerland) and were frame-by-frame motion corrected when necessary. The initial PET images (15 min) were averaged and aligned onto a rhesus or cynomolgus structural T1-weighted MRI template and the transformation matrix applied to the whole PET series. A volume of interest (VOI) atlas (including the caudate, putamen, globus pallidus, nucleus accumbens, thalamus, cortical regions, and cerebellum) was applied to the PET series in MRI rhesus or cynomolgus template space to extract the regional time activity curves. Curves were expressed in SUV (standardized uptake value) by normalizing the activity concentration by the injected dose and animal body weight.

Kinetic Modeling and Analysis. Time–activity curves were analyzed with one-tissue (1T) and two-tissue (2T) compartment models (18), and Logan graphical analysis (LGA) (19) using the arterial plasma input function corrected for radio-metabolites to derive the volume of distribution (V_T) and the influx rate constant K_1 in each region. The binding potential BP_{ND} was estimated using the cerebellum as reference region: $BP_{ND} = V_T/V_{ND} - 1$, V_T and V_{ND} being the distribution volumes in the target region (specific and non-displaceable binding) and reference region (non-displaceable binding), respectively (20). In addition, BP_{ND} was directly derived from the

Simplified Reference Tissue Model (SRTM) (21), and non-invasive Logan graphical analysis (NLGA) (19) with the cerebellum as reference region. All kinetic analyses were performed using PMOD 3.609. Test-retest variability for V_T and BP_{ND} was estimated as $ABS (test - retest) / AVERAGE (test + retest)$.

The D1R occupancy (Occ) produced by SCH-23390 or PF-2562 was determined as the percent change of BP_{ND} : $Occ = (BP_{ND}^{baseline} - BP_{ND}^{drug}) / BP_{ND}^{baseline}$. The SCH-23390 plasma-occupancy curves for the striatum (putamen and caudate) were fitted in GraphPad Prism (version 6.01, GraphPad Software, San Diego, CA, USA) with a single specific binding site model: $Occ = Occ_{max} \times C / (C + EC_{50})$, where Occ_{max} is the maximum occupancy, EC_{50} represents SCH-23390 plasma level for 50% occupancy and C represents SCH-23390 average plasma level during the scan.

¹⁸F-MNI-800 Whole-Body PET Studies

Two adult rhesus monkeys (*Macaca mulatta*), 1 male and 1 female, were used for whole-body PET imaging from head to mid-thigh over 4 hours on a Biograph mCT PET/CT camera (Siemens Healthcare Molecular Imaging, Knoxville, TN, USA) following intravenous bolus injection of ¹⁸F-MNI-800 to determine the biodistribution and estimate radiation absorbed doses.

PET images were imported into PMOD and VOIs were drawn on source organs. Radiation absorbed dose and effective dose (ICRP-60) were estimated with OLINDA/EXM 1.0 (Organ Level Internal Dose Assessment) software (22) according to the male or female model. ICRP-30 gastrointestinal model was used with the assumption that activity entered the gastrointestinal tract through the small intestine (fraction of activity entering the intestine was estimated as the highest fraction encountered in the intestinal area).

RESULTS

Plasma Analysis

HPLC analysis of ^{18}F -MNI-800 and ^{18}F -MNI-968 arterial plasma revealed one major radio-metabolite with one minor metabolite eluting just after the first one (whose contribution remained small throughout the study), with both metabolites more polar than the parent compound. No difference was observed between rhesus and cynomolgus macaques and the results were pooled across the two species. ^{18}F -MNI-800 and ^{18}F -MNI-968 showed similar moderate metabolic profile, with about 60-70% and 40-50% of intact parent remaining at 30 min and 120 min post injection respectively (Figure 3). Plasma parent f_p measured by ultrafiltration was $13.4 \pm 1.3 \%$ (n=4) for ^{18}F -MNI-800 and $13.5 \pm 1.5 \%$ (n=4) for ^{18}F -MNI-968.

Brain Uptake Distribution and Time Activity Curves

Representative average ^{18}F -MNI-968 and ^{18}F -MNI-800 PET images in a rhesus macaque at baseline show highest uptake in the striatum, consistent with known D1R distribution (Figure 4, left). ^{18}F -MNI-800 PET image after SCH-23390 pre-block (0.5 mg/kg) demonstrates almost complete saturation. ^{18}F -MNI-968 and ^{18}F -MNI-800 time-activity curves at baseline and after SCH-23390 (0.5 mg/kg) or PF-2562 (1.2 mg/kg) pre-block are presented in Figure 4 (right) in the same rhesus macaque. Both ^{18}F -MNI-968 and ^{18}F -MNI-800 readily entered the brain, with SUV peak uptake at 5–10 min after injection. Highest signal is noted in the putamen and caudate nucleus, followed by the globus pallidus and nucleus accumbens, with lowest uptake consistently found in the cerebellum. Clear blocking of ^{18}F -MNI-800 or ^{18}F -MNI-968 uptake is seen after pre-block with SCH-23390 (0.5 mg/kg, occupancy of ~85%) or PF-2562 (1.2 mg/kg, occupancy of

~40%), respectively. Higher uptake is also observed for ^{18}F -MNI-968 compared to ^{18}F -MNI-800 particularly in the putamen and caudate nucleus, while maintaining a similar profile in the cerebellum.

Kinetic Analysis

2T was favored for both ^{18}F -MNI-800 and ^{18}F -MNI-968 data over 1T based on the Akaike information criterion (data not shown). Typical 2T and SRTM fits as well as Logan plots (LGA with $t^*=15\text{min}$, and NI-LGA with $t^*=10\text{min}$) are provided in Figure 5 for a baseline study in rhesus macaque with ^{18}F -MNI-968. SRTM determined k'_2 to be $0.17 \pm 0.04 \text{ min}^{-1}$ ($n=4$) for ^{18}F -MNI-800 and $0.16 \pm 0.02 \text{ min}^{-1}$ ($n=5$) for ^{18}F -MNI-968, and these SRTM estimates of k'_2 were used for the NI-LGA fit.

Within-animal comparison ($n=2$) between ^{18}F -MNI-800 and ^{18}F -MNI-968 V_T estimates (2T model) is shown in Figure 6A, and indicates a higher specific signal for ^{18}F -MNI-968 (negative y-intercept) and same target/ B_{max} for both tracers (linearity of the relationship) (23). Since the free fraction f_p was similar for ^{18}F -MNI-800 and ^{18}F -MNI-968, the slope corresponds to the *in vivo* affinities ratio and predicts a dissociation constant K_D about 1.3 times higher for ^{18}F -MNI-800 (23). Furthermore, V_T in the cerebellum was $1.83 \pm 0.06 \text{ mL/cm}^3$ for ^{18}F -MNI-800 compared to $1.87 \pm 0.01 \text{ mL/cm}^3$ for ^{18}F -MNI-968, demonstrating a similar non-displaceable signal for both tracers, with a relationship for the binding potential BP_{ND} (2T model) for the within-animal studies: $BP_{ND}(\text{MNI-968}) = 1.29 \times BP_{ND}(\text{MNI-800}) + 0.006$.

Figure 6B and 6C show comparison of V_T and BP_{ND} across methods for ^{18}F -MNI-968, demonstrating very good agreement between the different estimates ($R^2=0.99$), in particular for BP_{ND} between plasma-based and reference region-based methods, with points lining almost on the

identity line. Similar results were obtained for ^{18}F -MNI-800 (data not shown). A summary of V_T and BP_{ND} for the different methods is provided in a subset of regions in Table 2 for ^{18}F -MNI-800 (n=4) and in Table 3 for ^{18}F -MNI-968 (n=3 for 2T and LGA, and n=5 for SRTM and NI-LGA). Additional kinetic parameters for 2T are provided in Supplemental Tables 1-2. V_T ranged from $\sim 1.9 \pm 0.1 \text{ mL/cm}^3$ in the cerebellum (similar estimates for both tracers) to $\sim 3.7 \pm 0.3 \text{ mL/cm}^3$ and $\sim 4.3 \pm 0.2 \text{ mL/cm}^3$ in the putamen for ^{18}F -MNI-800 and ^{18}F -MNI-968, respectively. BP_{ND} ranged from ~ 0.2 in the cortex to ~ 0.9 in the putamen for ^{18}F -MNI-800, and from ~ 0.3 in the cortex to ~ 1.1 - 1.2 in the putamen for ^{18}F -MNI-968, confirming an average specific signal higher by $\sim 30\%$. K_1 (2T model) was similar across regions, animals, and tracers with $K_1 = 0.23 \pm 0.03 \text{ mL}\cdot\text{cm}^{-3}\cdot\text{min}^{-1}$ for ^{18}F -MNI-800 and $K_1 = 0.27 \pm 0.06 \text{ mL}\cdot\text{cm}^{-3}\cdot\text{min}^{-1}$ for ^{18}F -MNI-968 (Supplemental Tables 1-2).

Test-retest variability was assessed in a limited number of repeat studies for ^{18}F -MNI-800 (n=2) and ^{18}F -MNI-968 (n=1). Results are summarized in Supplemental Tables 3-4 for the different methods used. Variability of V_T estimates was low in all regions and both tracers ($< 10\%$), while that of BP_{ND} in the striatum remained low for ^{18}F -MNI-800 ($< 5\%$) and somewhat higher for ^{18}F -MNI-968 ($\sim 15\%$) for which however test and retest scans were separated by 4 months.

SCH-23390 Occupancy Studies

Pre-blocking with SCH-23390 increased the measured occupancies in a dose-dependent fashion, and reduced the ^{18}F -MNI-800 uptake to levels close to those in the cerebellum at the highest dose tested (Figure 4), supporting the specificity and selectivity of ^{18}F -MNI-800 for D1R, with measured occupancies of $\sim 85\%$ and $\sim 60\%$ at the two highest SCH-23390 doses of 0.5 and 0.2 mg/kg, respectively.

SCH-23390 plasma levels during the pre-block studies are shown in Figure 7A, and the relationship between the measured D1R occupancy and the average plasma levels during the PET imaging (25 to 145 min post administration of SCH-23390) is shown in Figure 7B for the various analysis methods used, where the maximum occupancy was constrained to 100%. All methods produced similar occupancy measurements, with slightly lower estimates for 2T at the two lowest SCH-23390 doses, with consistent estimated EC₅₀ ranging from 6.0 ± 1.0 ng/mL for NI-LGA to 8.5 ± 1.0 ng/mL for 2T (average ~7 ng/mL).

¹⁸F-MNI-800 Dosimetry

Whole-body studies showed that the elimination of ¹⁸F-MNI-800 takes place mainly via the hepatobiliary route. The urinary bladder, gallbladder and liver were determined to be the critical organs with the highest absorbed dose (Supplemental Table 5). The whole-body effective dose (ED) was estimated to be 0.025 mSv/MBq for the female and 0.021 mSv/MBq for the male rhesus, in line with other ¹⁸F-labelled tracers (e.g. 0.019 mSv/MBq for fluorodeoxyglucose ¹⁸F-FDG (24)).

DISCUSSION

Both ¹⁸F-MNI-800 and its active atropisomeric (-)-enantiomer ¹⁸F-MNI-968 demonstrated high brain penetration in monkey brain with uptake distribution in agreement with the known D1R distribution. Blood profiles were highly similar, with almost identical metabolism rate and free fraction *f_p* (~13%).

SCH-23390 has a 5-HT_{2a} component (15), however the density of 5-HT_{2a} receptors in the striatum is negligible compared to D1R. Therefore, SCH-23390 pre-blocking studies confirmed

the specificity and selectivity of ^{18}F -MNI-800 for D1R over other targets in the striatum, which is expected to hold true for ^{18}F -MNI-968 as it is one enantiomer. Absolute selectivity against 5-HT_{2a} receptors could be tested further by a challenge with the selective 5-HT_{2a} antagonist MDL 100907. These studies also confirmed the choice of the cerebellum as a reference region for non-invasive methods, BP_{ND} calculations and occupancy measurements since the signal in this region was not blocked. This is also supported by a V_{ND} estimate from occupancy plots of 2.0 ± 0.1 (data not shown) (25), in very good agreement with V_{T} of 1.9 ± 0.1 in the cerebellum (Table 2). Assuming passive diffusion through the blood brain barrier, the tissue free fraction can be calculated from the measured f_{p} and V_{ND} above (20), giving $f_{\text{ND}} \sim 7\%$, in close agreement with cF_{u_b} of 6%. Finally, the agreement in the occupancy estimates between the plasma-based and reference-region-based methods suggests that D1R occupancy can be quantitatively assessed in monkeys using SRTM or NI-LGA, without the need for arterial sampling.

BP_{ND} in human and NHP was reported to be ~ 0.4 - 0.6 in the cortex and ~ 2.0 - 3.0 in the striatum for ^{11}C -SCH-23390 and ~ 0.6 - 0.8 in the cortex and ~ 3.0 - 4.0 in the striatum for ^{11}C -NNC-112 (15,26-28), which is higher than the values reported here for ^{18}F -MNI-968 (~ 0.3 in the cortex and ~ 1.1 in the striatum, Table 3). Also, BP_{ND} variability in humans was reported as ~ 10 - 15% in the cortex and ~ 5.0 - 10% in the striatum for both ^{11}C -SCH-23390 and ^{11}C -NNC-112 (27,29), marginally better than that reported here (Supplemental Table 3), although we assessed the variability in a limited number of animals. However, both ^{11}C -SCH-23390 and ^{11}C -NNC-112 are antagonist radioligands, and cannot therefore provide information regarding the high or low affinity state of D1R, and both suffer from a 5-HT_{2a} signal in the cortex which represents about 20-30% of the total signal (15,26). Therefore, further evaluation and characterization of ^{18}F -MNI-

968 in human subjects is warranted as the tracer could prove to be a valuable tool in Parkinson's disease (9) and in psychiatric disorders such as schizophrenia (8).

CONCLUSION

We report herein the evaluation of racemate ^{18}F -MNI-800 and its (-)-enantiomer ^{18}F -MNI-968 in NHP. Both tracers had regional uptake consistent with D1R distribution. The selectivity and specificity of ^{18}F -MNI-800 and ^{18}F -MNI-968 for D1R were demonstrated against SCH-23390 or PF-2562, selective D1R antagonist and partial agonist, respectively. Non-invasive quantification of ^{18}F -MNI-800 and ^{18}F -MNI-968 with SRTM or Logan graphical analysis using the cerebellum as a reference is possible, particularly for occupancy studies. ^{18}F -MNI-800 dosimetry, and putatively that of ^{18}F -MNI-968, is favorable, with an effective dose consistent with values reported for other PET radiotracers. Therefore, ^{18}F -MNI-968 (^{18}F -PF-0110) has great potential as a D1R agonist PET radiotracer and warrants further characterization in human subjects.

KEY POINTS

Question: Does agonist PET tracer ^{18}F -MNI-968 show suitable properties and specific binding to quantify D1 dopamine receptor?

Pertinent Findings: ^{18}F -MNI-968, the atropisomeric (-)-enantiomer, showed suitable in vitro pharmacology profile, high brain uptake, favorable kinetics and specific binding that was blocked by selective D1R antagonist and partial agonist.

Implications for Patient Care: ^{18}F -MNI-968 has potential as an agonist PET radioligand to quantify D1 receptors in high affinity state in human brains, particularly in neurological and psychiatric disorders.

DISCLOSURE

The research reported in this publication was supported by the National Institute of Mental Health of the National Institutes of Health under Award Number U01MH107803. No other potential conflicts of interest relevant to this article exist.

ACKNOWLEDGMENTS

The authors thank Dr. Richard Carson and the staff at the Yale PET Center for conducting the rhesus monkey experiments.

REFERENCES

1. Hall H, Sedvall G, Magnusson O, Kopp J, Halldin C, Farde L. Distribution of D1- and D2-dopamine receptors, and dopamine and its metabolites in the human brain. *Neuropsychopharmacology*. 1994;11:245-256.
2. Meador-Woodruff JH, Damask SP, Wang J, Haroutunian V, Davis KL, Watson SJ. Dopamine receptor mRNA expression in human striatum and neocortex. *Neuropsychopharmacology*. 1996;15:17-29.
3. Rosell DR, Zaluda LC, McClure MM, et al. Effects of the D1 dopamine receptor agonist dihydrexidine (DAR-0100A) on working memory in schizotypal personality disorder. *Neuropsychopharmacology*. 2015;40:446-453.
4. Schneider JS, Sun ZQ, Roeltgen DP. Effects of dihydrexidine, a full dopamine D-1 receptor agonist, on delayed response performance in chronic low dose MPTP-treated monkeys. *Brain Res*. 1994;663:140-144.
5. Kozak R, Kiss T, Dlugolenski K, et al. Characterization of PF-6142, a novel, non-catecholamine dopamine receptor D1 agonist, in murine and nonhuman primate models of dopaminergic activation. *Front Pharmacol*. 2020;11:1005.

6. Hall A, Provins L, Valade A. Novel strategies to activate the dopamine D1 receptor: recent advances in orthosteric agonism and positive allosteric modulation. *J Med Chem.* 2019;62:128-140.
7. Coe JW, Allen JA, Davoren JE, et al. Heteroaromatic compounds and their use as dopamine D1 ligands. *PCT Int Appl.* 2014;WO 2014072881 A1.
8. Arce E, Balice-Gordon R, Duvvuri S, et al. A novel approach to evaluate the pharmacodynamics of a selective dopamine D1/D5 receptor partial agonist (PF-06412562) in patients with stable schizophrenia. *J Psychopharmacol.* 2019;33:1237-1247.
9. Papapetropoulos S, Liu W, Duvvuri S, Thayer K, Gray DL. Evaluation of D1/D5 partial agonist PF-06412562 in Parkinson's disease following oral administration. *Neurodegener Dis.* 2018;18:262-269.
10. Halldin C, Foged C, Chou YH, et al. Carbon-11-NNC 112: a radioligand for PET examination of striatal and neocortical D1-dopamine receptors. *J Nucl Med.* 1998;39:2061-2068.

11. Halldin C, Stone-Elander S, Farde L, et al. Preparation of ¹¹C-labelled SCH 23390 for the in vivo study of dopamine D-1 receptors using positron emission tomography. *Int J Rad Appl Instrum A*. 1986;37:1039-1043.

12. Kassiou M, Scheffel U, Ravert HT, et al. [¹¹C]A-69024: a potent and selective non-benzazepine radiotracer for in vivo studies of dopamine D1 receptors. *Nucl Med Biol*. 1995;22:221-226.

13. Finnema SJ, Bang-Andersen B, Jorgensen M, et al. The dopamine D(1) receptor agonist (S)-[¹¹C]N-methyl-NNC 01-0259 is not sensitive to changes in dopamine concentration--a positron emission tomography examination in the monkey brain. *Synapse*. 2013;67:586-595.

14. Palner M, McCormick P, Parkes J, Knudsen GM, Wilson AA. Systemic catechol-O-methyl transferase inhibition enables the D1 agonist radiotracer R-[¹¹C]SKF 82957. *Nucl Med Biol*. 2010;37:837-843.

15. Ekelund J, Slifstein M, Narendran R, et al. In vivo DA D(1) receptor selectivity of NNC 112 and SCH 23390. *Mol Imaging Biol*. 2007;9:117-125.

16. Zhang L, Villalobos A, Beck EM, et al. Design and selection parameters to accelerate the discovery of novel central nervous system positron emission tomography (PET) ligands and their application in the development of a novel phosphodiesterase 2A PET ligand. *J Med Chem.* 2013;56:4568-4579.

17. Cumming P. Absolute abundances and affinity states of dopamine receptors in mammalian brain: A review. *Synapse.* 2011;65:892-909.

18. Slifstein M, Laruelle M. Models and methods for derivation of in vivo neuroreceptor parameters with PET and SPECT reversible radiotracers. *Nucl Med Biol.* 2001;28:595-608.

19. Logan J. A review of graphical methods for tracer studies and strategies to reduce bias. *Nucl Med Biol.* 2003;30:833-844.

20. Innis RB, Cunningham VJ, Delforge J, et al. Consensus nomenclature for in vivo imaging of reversibly binding radioligands. *J Cereb Blood Flow Metab.* 2007;27:1533-1539.

21. Lammertsma AA, Hume SP. Simplified reference tissue model for PET receptor studies. *Neuroimage.* 1996;4:153-158.

22. Stabin MG, Sparks RB, Crowe E. OLINDA/EXM: the second-generation personal computer software for internal dose assessment in nuclear medicine. *J Nucl Med.* 2005;46:1023-1027.

23. Guo Q, Owen DR, Rabiner EA, Turkheimer FE, Gunn RN. A graphical method to compare the in vivo binding potential of PET radioligands in the absence of a reference region: application to [(1)(1)C]PBR28 and [(1)(8)F]PBR111 for TSPO imaging. *J Cereb Blood Flow Metab.* 2014;34:1162-1168.

24. Delbeke D, Coleman RE, Guiberteau MJ, et al. Procedure guideline for tumor imaging with 18F-FDG PET/CT 1.0. *J Nucl Med.* 2006;47:885-895.

25. Cunningham VJ, Rabiner EA, Slifstein M, Laruelle M, Gunn RN. Measuring drug occupancy in the absence of a reference region: the Lassen plot re-visited. *J Cereb Blood Flow Metab.* 2010;30:46-50.

26. Slifstein M, Kegeles LS, Gonzales R, et al. [11C]NNC 112 selectivity for dopamine D1 and serotonin 5-HT(2A) receptors: a PET study in healthy human subjects. *J Cereb Blood Flow Metab.* 2007;27:1733-1741.
27. Abi-Dargham A, Martinez D, Mawlawi O, et al. Measurement of striatal and extrastriatal dopamine D1 receptor binding potential with [11C]NNC 112 in humans: validation and reproducibility. *J Cereb Blood Flow Metab.* 2000;20:225-243.
28. Kosaka J, Takahashi H, Ito H, et al. Decreased binding of [11C]NNC112 and [11C]SCH23390 in patients with chronic schizophrenia. *Life Sci.* 2010;86:814-818.
29. Hirvonen J, Nagren K, Kajander J, Hietala J. Measurement of cortical dopamine d1 receptor binding with 11C[SCH23390]: a test-retest analysis. *J Cereb Blood Flow Metab.* 2001;21:1146-1150.

FIGURES

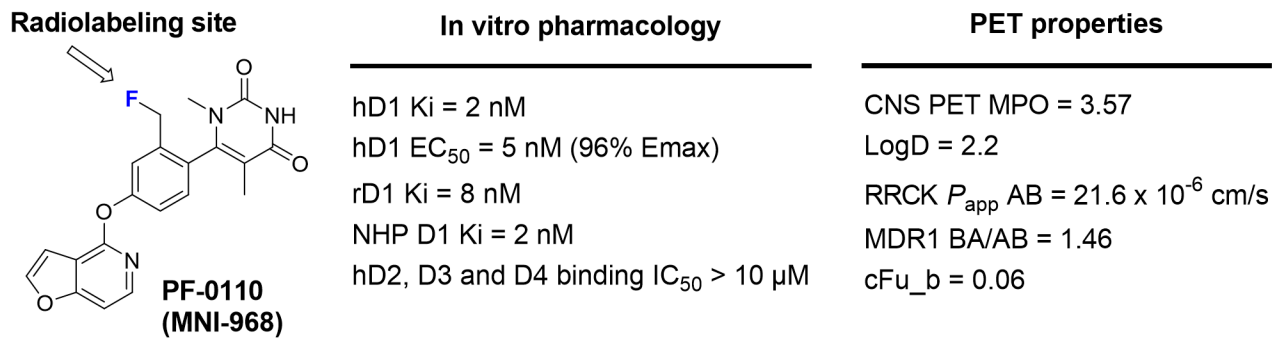


FIGURE 1: Profile of D1R agonist PET ligand lead PF-0110 (MNI-968).

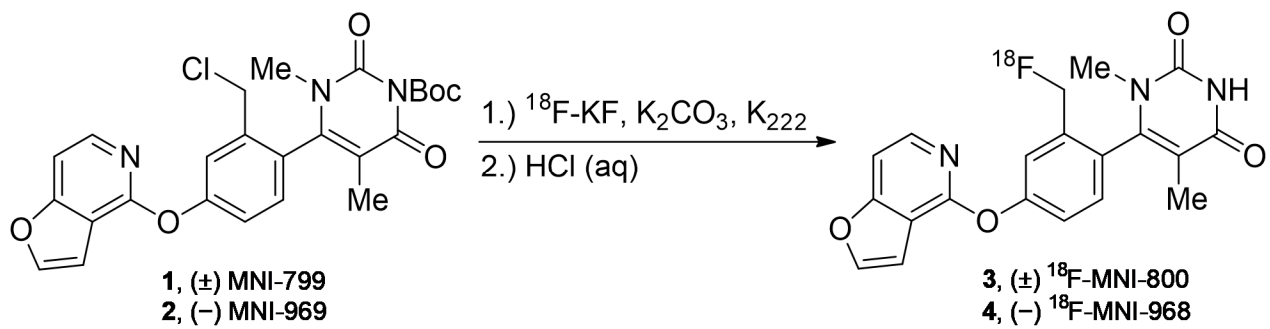


FIGURE 2: Radiosynthesis of ^{18}F -MNI-800 (^{18}F -PF-8477) and ^{18}F -MNI-968 (^{18}F -PF-0110).

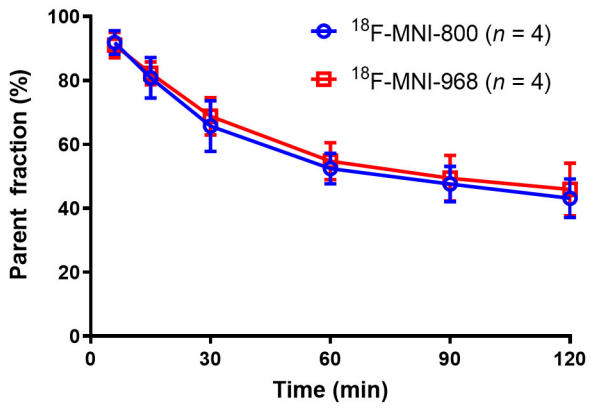


FIGURE 3: Parent fraction profile in arterial plasma after intravenous administration of ¹⁸F-MNI-800 (mean ± SD, n = 4) or ¹⁸F-MNI-968 (mean ± SD, n = 4).

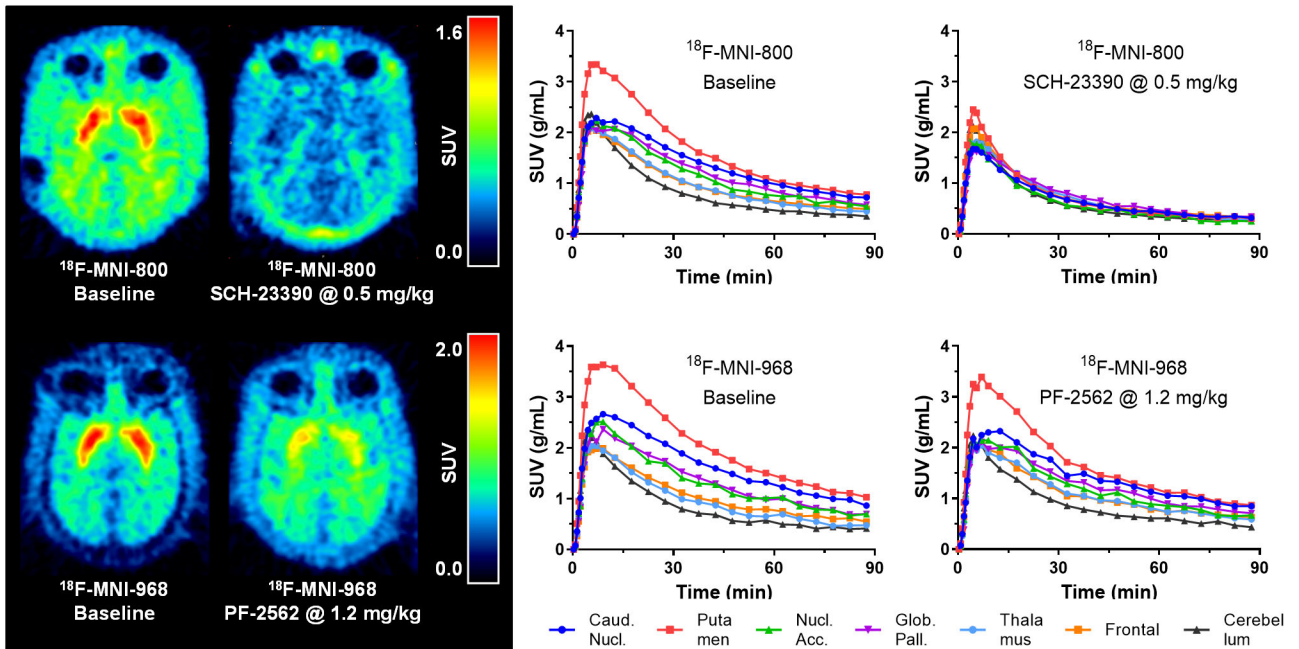


FIGURE 4: Left: average PET images from 30-90 min post-injection for a rhesus macaque (NHP A) in transverse plane of ^{18}F -MNI-800 (top row) at baseline and post-dosing with SCH-23390 at 0.5 mg/kg (occupancy of ~85%) and of ^{18}F -MNI-968 (bottom row) at baseline and post-dosing with PF-2562 at 1.2 mg/kg (occupancy of ~40%). Right: time activity curves in some brain regions for the same rhesus macaque for the studies with ^{18}F -MNI-800 (top row) and ^{18}F -MNI-968 (bottom row).

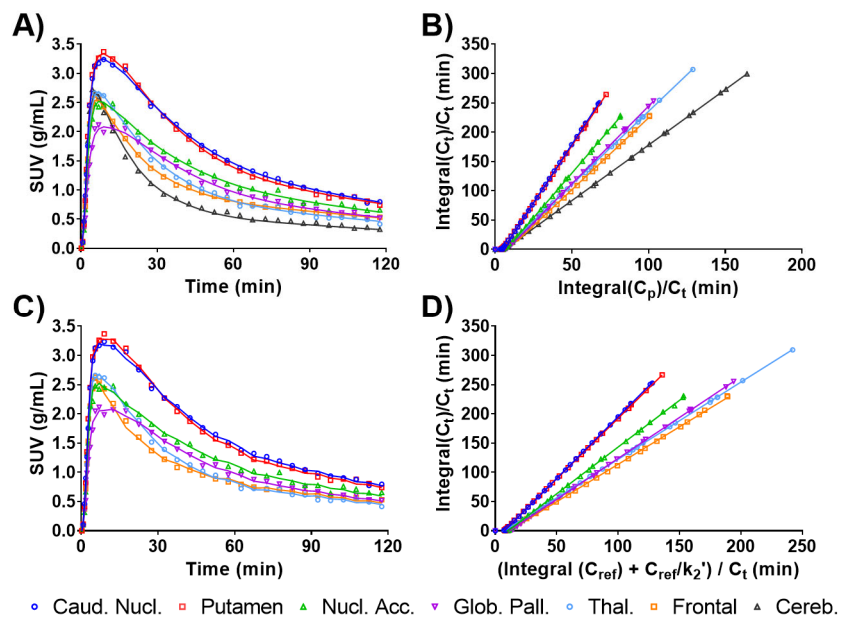


FIGURE 5: Representative time activity curves at baseline for a rhesus macaque (NHP B) in some brain regions following bolus injection of ^{18}F -MNI-968, showing (A) 2T compartment model fits and (C) SRTM fits. Graphical analysis with (B) LGA with plasma input function ($t^*=15$ min) and (D) NI-LGA with reference region input function ($t^*=10$ min).

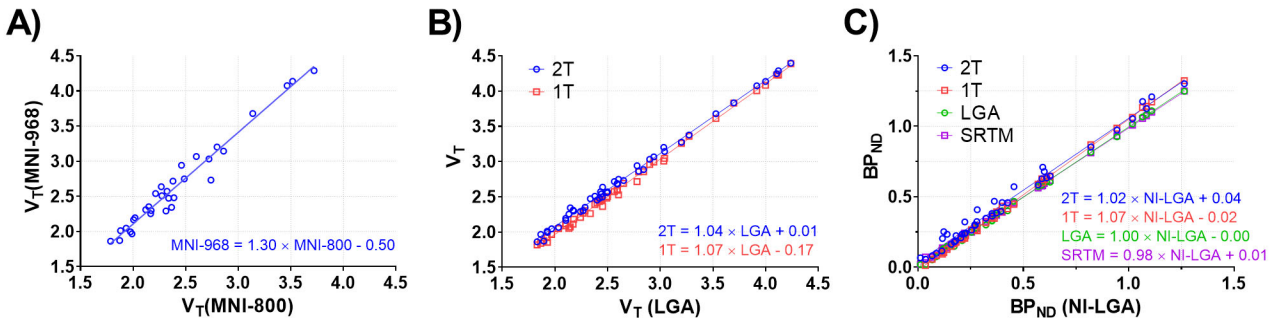


FIGURE 6: (A) Within-animal comparison (n=2) of ^{18}F -MNI-800 and ^{18}F -MNI-968 2T V_T estimates. (B) Comparison of ^{18}F -MNI-968 V_T estimates across models (n=3). (C) Comparison of ^{18}F -MNI-968 BP_{ND} estimates across models (n=3).

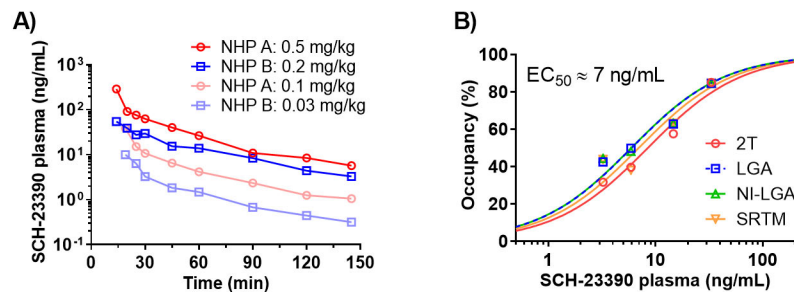


FIGURE 7: (A) SCH-23390 plasma levels for the four doses, with ^{18}F -MNI-800 injection at 25 min post drug administration. (B) Striatal D_1 receptor occupancy against average plasma levels between 25-145 min post administration of SCH-23390.

TABLES

TABLE 1. Summary of scans with ^{18}F -MNI-800 or ^{18}F -MNI-968.

NHP		^{18}F -MNI-800 (scans of 120 min)	^{18}F -MNI-968 (scans of 120 or *90 min)
Rhesus:	A	Test, Retest, SCH23390 (0.5 and 0.1 mg/kg)	Test, *Retest, *PF-2562 (1.2 mg/kg)
	B	Test, Retest, SCH23390 (0.2 and 0.03 mg/kg), Dosimetry	Baseline
	C	Dosimetry	*Baseline, *PF-2562 (1.2 mg/kg)
Cynomolgus:	D	Baseline	Baseline
	E	Baseline	
	F		Baseline

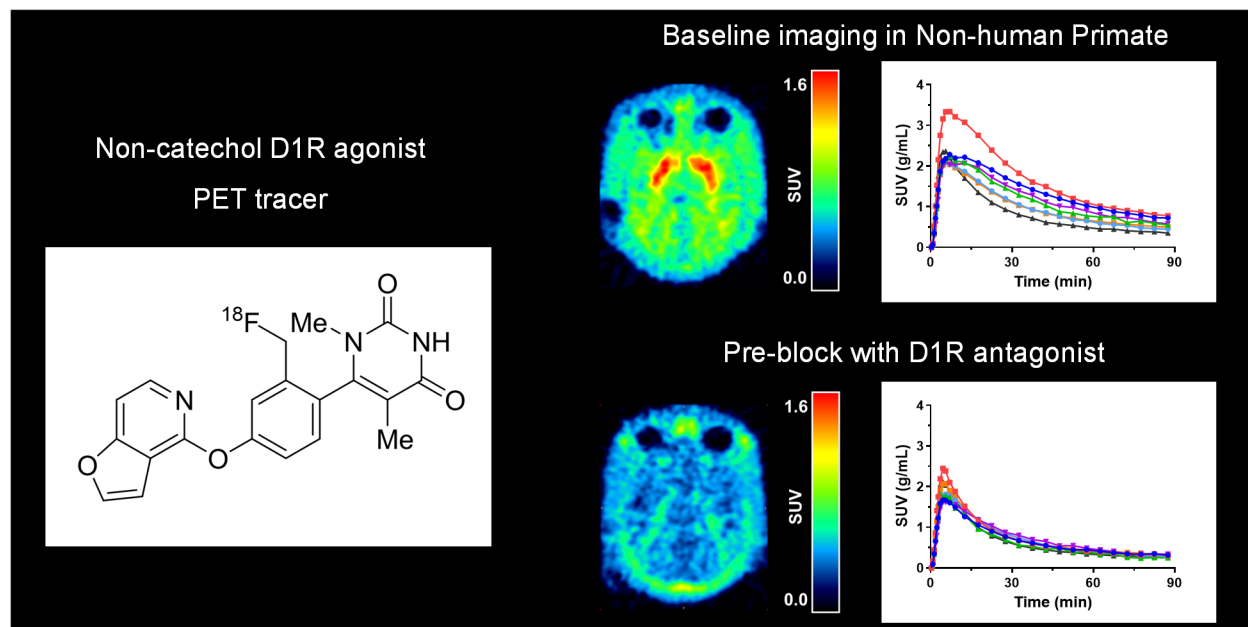
TABLE 2. ^{18}F -MNI-800 V_T and BP_{ND} in pooled rhesus and cynomolgus macaques ($n = 4$, mean \pm standard deviation (cov)).

Region	V_T		BP_{ND}			
	2T	LGA	2T	LGA	SRTM	NI-LGA
Striatum	3.6 ± 0.3	3.5 ± 0.3	0.86 ± 0.10	0.83 ± 0.08	0.83 ± 0.07	0.83 ± 0.07
	(8%)	(8%)	(11%)	(9%)	(8%)	(8%)
Caudate	3.5 ± 0.4	3.4 ± 0.4	0.81 ± 0.11	0.78 ± 0.10	0.78 ± 0.09	0.78 ± 0.09
	(11%)	(11%)	(14%)	(12%)	(11%)	(12%)
Putamen	3.7 ± 0.3	3.6 ± 0.3	0.91 ± 0.14	0.88 ± 0.12	0.89 ± 0.11	0.89 ± 0.11
	(7%)	(7%)	(15%)	(13%)	(12%)	(13%)
Nucleus accumbens	2.9 ± 0.2	2.8 ± 0.2	0.48 ± 0.03	0.46 ± 0.02	0.45 ± 0.02	0.46 ± 0.02
	(7%)	(7%)	(6%)	(5%)	(5%)	(5%)
Globus pallidus	2.9 ± 0.3	2.8 ± 0.3	0.50 ± 0.06	0.48 ± 0.06	0.48 ± 0.06	0.48 ± 0.05
	(9%)	(9%)	(13%)	(12%)	(12%)	(11%)
Thalamus	2.4 ± 0.2	2.4 ± 0.2	0.25 ± 0.06	0.25 ± 0.04	0.26 ± 0.04	0.26 ± 0.04
	(9%)	(8%)	(22%)	(17%)	(16%)	(16%)
Frontal cortex	2.3 ± 0.0	2.2 ± 0.0	0.24 ± 0.04	0.20 ± 0.05	0.20 ± 0.05	0.20 ± 0.05
	(0%)	(1%)	(18%)	(24%)	(23%)	(25%)
Cerebellum	1.9 ± 0.1	1.9 ± 0.1				
	(7%)	(6%)				

TABLE 3. ^{18}F -MNI-968 V_T and BP_{ND} in pooled rhesus and cynomolgus macaques (n = 3 for 2T and LGA, and n=5 for SRTM and NI-LGA, mean \pm standard deviation (cov)).

Region	V_T		BP_{ND}			
	2T	LGA	2T	LGA	SRTM	NI-LGA
Striatum	4.1 ± 0.2	4.0 ± 0.2	1.14 ± 0.05	1.07 ± 0.02	1.07 ± 0.03	1.08 ± 0.03
	(4%)	(4%)	(5%)	(2%)	(2%)	(3%)
Caudate	4.0 ± 0.3	3.9 ± 0.3	1.08 ± 0.12	1.02 ± 0.09	1.06 ± 0.09	1.06 ± 0.08
	(8%)	(8%)	(11%)	(9%)	(8%)	(8%)
Putamen	4.3 ± 0.2	4.1 ± 0.2	1.20 ± 0.09	1.13 ± 0.10	1.11 ± 0.08	1.12 ± 0.08
	(4%)	(4%)	(8%)	(9%)	(7%)	(8%)
Nucleus accumbens	3.2 ± 0.2	3.1 ± 0.2	0.65 ± 0.02	0.61 ± 0.00	0.59 ± 0.07	0.60 ± 0.07
	(5%)	(6%)	(4%)	(0%)	(12%)	(12%)
Globus pallidus	3.2 ± 0.6	3.1 ± 0.5	0.65 ± 0.20	0.60 ± 0.21	0.58 ± 0.18	0.58 ± 0.18
	(18%)	(18%)	(31%)	(35%)	(31%)	(31%)
Thalamus	2.6 ± 0.2	2.6 ± 0.2	0.35 ± 0.04	0.33 ± 0.04	0.29 ± 0.05	0.29 ± 0.06
	(9%)	(9%)	(13%)	(13%)	(19%)	(20%)
Frontal cortex	2.6 ± 0.1	2.4 ± 0.1	0.33 ± 0.08	0.27 ± 0.04	0.28 ± 0.05	0.28 ± 0.05
	(2%)	(2%)	(25%)	(15%)	(17%)	(18%)
Cerebellum	1.9 ± 0.1	1.9 ± 0.1				
	(6%)	(5%)				

GRAPHICAL ABSTRACT

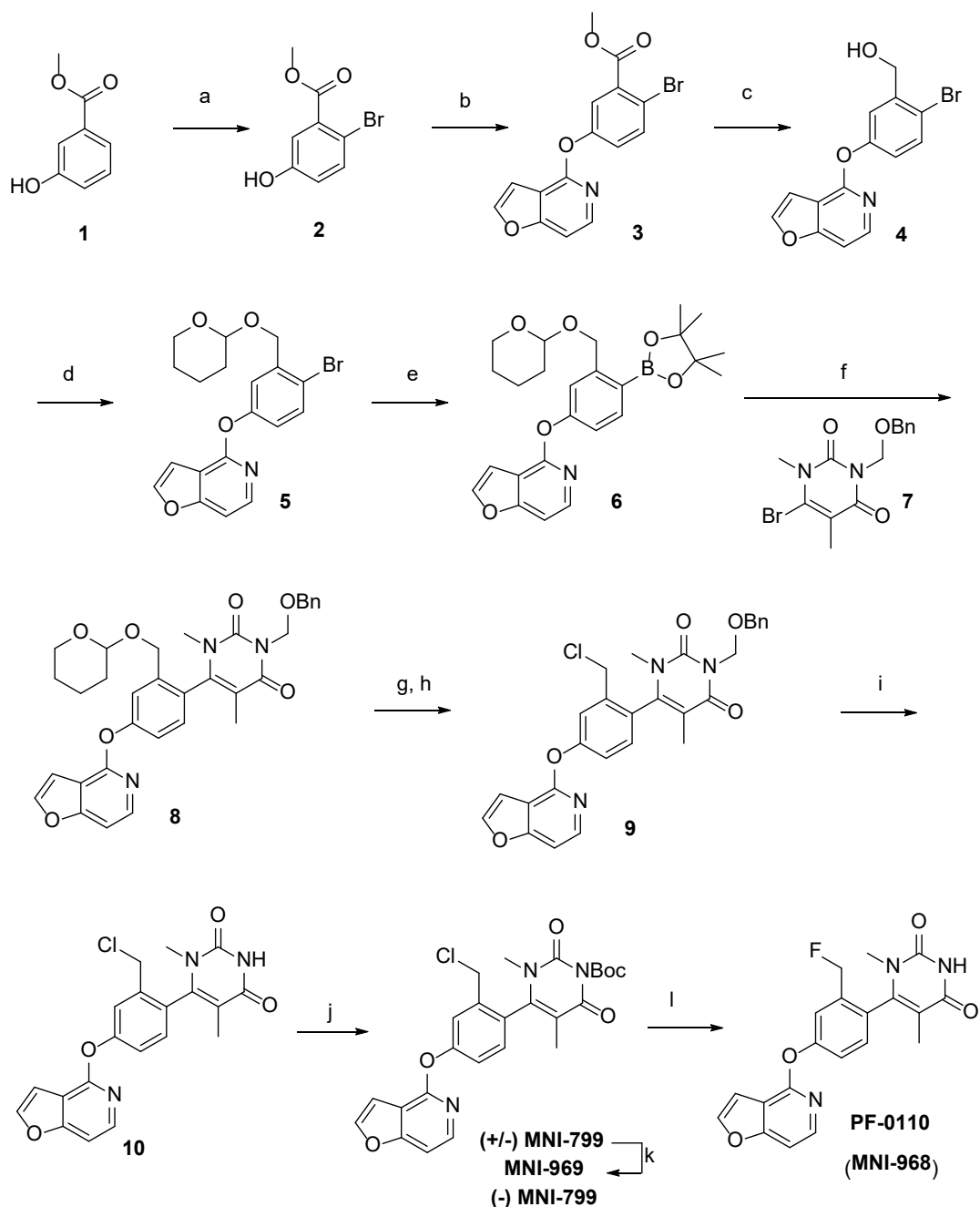


SUPPLEMENTAL MATERIALS

Synthesis of MNI-968 (PF-0110) and MNI-800 (PF-8477) and their precursor MNI-969 and MNI-799, respectively

The synthetic route used to prepare MNI-968 (PF-0110) and its corresponding labeling precursor MNI-969 is illustrated in Scheme 1. The synthesis of the precursor MNI-969 involves ten steps starting from commercially available methyl 3-hydroxybenzoate (**1**). Bromination using bromine at room temperature in dichloromethane provided compound **2** in 99% yield. The subsequent S_NAr reaction with 4-chlorofurano[3,2-*c*]pyridine yielded ester **3**, which upon reduction using lithium borohydride provided the corresponding benzyl alcohol **4**. THP protection was successfully achieved in high yield (99%) by treating compound **4** with 3,4-dihydro-2H-pyran in the presence of *p*-toluenesulfonic acid monohydrate. The resulted compound **5** was then converted to boronic ester **6**, which was subsequently subjected to coupling reaction with benzyloxy methyl (BOM) protected bromouracil **7** to give the desired product **8**. Selective removal of the THP protecting group by 4N HCl in 1,4-dioxane and the resulted benzyl alcohol was converted to the corresponding benzyl chloride **9** in nearly quantitative yield. The BOM protecting group was then removed using a two-step procedure involving treatment with BCl_3 in dichloromethane from -78 °C to room temperature, followed by 1N HCl in 1,4-dioxane at 80 °C. The resulted uracil **10** was re-protected by the Boc group to give MNI-799, the racemic precursor of MNI-800 (PF-8477). Chiral separation of the two atropisomers was achieved using the condition detailed in Supplemental Scheme 1 to yield the desired atropisomer MNI-969 as a white solid with an optical rotation of -6.6 degrees and chiral purity of 98.15%. Finally, MNI-969 was converted to MNI-968 in one-step upon treatment with potassium fluoride in DMSO at 120 °C for 10 min, confirming the viability of late-stage fluorination as a radiolabeling strategy.

Supplemental SCHEME 1: Synthesis of MNI-968 and its radiolabeling precursor MNI-969



Reagents and conditions: a) Br₂, DCM, rt, 99%; b) 4-Chlorofurano[3,2-c]pyridine, Cs₂CO₃, DMSO, 80 °C, then addition of MeI, rt, 53%; c) LiBH₄, THF, 65 °C, 81%; d) 3,4-DHP, *p*-TsOH, DCM, rt, 99%; e) bis(pinacolato)diboron, Pd(dppf)Cl₂, KOAc, 1,4-dioxane, 100 °C, 85%; f) compound 7, Pd(dppf)Cl₂, 3M K₂CO₃ aqueous solution, 1,4-dioxane, 71%; g) 4N HCl in 1,4-dioxane, DCM, rt, 63%; h) SOCl₂, DCM, rt, 99%; i) BCl₃, DCM, -78 °C to rt, then 1N HCl, 1,4-dioxane, 80 °C, 99%; j) Boc₂O, Et₃N, DMAP, THF, rt; k) chiral separation using the following condition. Column: Chiral Tech IC 250mm x 21.2 mm 5 micron; Isocratic Conditions: mobile phase A, 80% CO₂; mobile phase B, 20% 75:25:0.2% MeOH: EtOAc: ammonia; Flow rate: 80.0 mL/min; l) KF, kryptofix, DMSO, 120 °C, 43%.

Radiochemistry of ^{18}F -MNI-800 (^{18}F -PF-8477) and ^{18}F -MNI-968 (^{18}F -PF-0110)

Materials: Components and reagents used for the radiolabeling were obtained from the following sources: Acetonitrile anhydrous (Sigma-Aldrich, part # 271004), Acetonitrile HPLC (Sigma-Aldrich, part # 34998), Sep-Pak QMA (ABX, part # K-925), Potassium carbonate (Sigma-Aldrich, part # 367877), Kryptofix 222 (ABX, part # 8000.1000), Dimethylsulfoxide anhydrous (Sigma-Aldrich, part # 276855), Hydrochloric acid (Sigma-Aldrich, part # 1.09057), Ethanol 200 Proof (Pharco-Aaper, part # 111000200), Water HPLC (Sigma-Aldrich, part # 270733), triethylamine (Sigma-Aldrich, part # 471283), Ammonium acetate (Sigma-Aldrich, part # 17836), Sodium ascorbate (Mylan, part # NDC 67457-118-50), Sep-Pak tC18 (Waters, part # WAT036805), Sep-Pak Oasis HLB light (Waters, part # 186005125), Methanol HPLC (Sigma-Aldrich, part # 34860), Saline 0.9% (Hospira, part # NDC0409488806), Water for injection (Hospira, part # NDC04094887-24), Filter 0.2-0.22 μm (Millipore, part # SLLG013SL), Sterile vial (Hospira, part # 5816-31).

^{18}F -MNI-800 (3): In a typical procedure, ^{18}F -fluoride in a shipping vial (target water obtained from a cyclotron facility) is transferred onto and trapped on a Sep-Pak QMA light ion exchange cartridge. It is then eluted with an aqueous acetonitrile solution (1 mL) of potassium carbonate (1.25 mg) and Kryptofix 222 (10 mg) into the reaction vessel of the TRACERlab® module. The solution is first evaporated by heating at 95°C for 4 min under vacuum and helium flow. Acetonitrile (1 mL) is added to the reactor and the evaporation is continued under the same conditions for 2 min under vacuum. After a second addition of acetonitrile (1 mL), final evaporation is carried out at 95°C for 2 min under vacuum and helium flow. The reactor is then cooled to 50°C. A solution of the precursor MNI-799 (1, 1.0 mg) in anhydrous dimethylsulfoxide

(1.0 mL) is added to the reaction vessel and the reaction mixture is heated at 80°C for 5 min. After 5 min, the reactor is cooled to 70°C, hydrochloric acid (1M, 1.0 mL) is added and heated at 70°C for 5 min before being cooled to 40°C. The mixture is transferred to the HPLC loading vial. The reactor is rinsed with HPLC mobile phase (2.0 mL) and transferred to the HPLC loading vial, pre-filled with NaOH (1M, 1.1 mL). The entire contents of vial are transferred into the HPLC injector loop for purification. Purification is performed by column with a Phenomenex Luna C18 (2) (10 µm, 250 x10 mm) and eluted with a mixture of ethanol/water/triethyl amine solution (30/70/0.1 v/v/v) at a flow rate of 4 mL/min. The product fraction is collected into the collection flask, containing 25 mL of ascorbic acid (10 mg/mL) in WFI. The diluted product mixture is passed through a tC18 solid-phase extraction cartridge and the cartridge is rinsed with 10 mL of ascorbic acid (10 mg/mL) in WFI. The radiolabeled product is eluted from the SPE cartridge with 1 mL of 200-proof USP grade ethanol into the formulation flask, pre-loaded with 10 mL of formulation base (ascorbic acid (0.7 mg/mL) in 0.9% saline). The cartridge is rinsed with 4 mL of formulation base and the rinse is mixed with the contents of the formulation flask. The resulting solution is passed through a sterilizing 0.2 µm membrane filter into a sterile, filter-vented vial (final product vial, FPV), pre-filled with 15 mL of saline.

¹⁸F-MNI-968 (4): In a typical procedure, ¹⁸F-fluoride in a shipping vial (target water obtained from a cyclotron facility) is transferred onto and trapped on a Sep-Pak QMA light ion exchange cartridge. It is then eluted with an aqueous acetonitrile solution (1 mL) of potassium carbonate (1.25 mg) and Kryptofix 222 (10 mg) into the reaction vessel of the TRACERlab® module. The solution is first evaporated by heating at 95°C for 4 min under vacuum and helium flow. Acetonitrile (1 mL) is added to the reactor and the evaporation is continued under the same

conditions for 2 min under vacuum. After a second addition of acetonitrile (1 mL), final evaporation is carried out at 95°C for 2 min under vacuum and helium flow. The reactor is then cooled to 50°C. A solution of the precursor MNI-969 (**2**, 0.7 mg) in anhydrous acetonitrile (0.7 mL) is added to the reaction vessel and the reaction mixture is heated at 80°C for 5 min. After 5 min, the reactor is cooled to 70°C, hydrochloric acid (1M, 0.8 mL) is added and heated at 70°C for 4 min before being cooled to 40°C and diluted with water for injection (WFI) (10 mL). The mixture is transferred from the reactor onto an intermediate solid phase extraction cartridge (SPE, Oasis HLB light). The reactor is rinsed with methanol (2.0 mL) and transferred through SPE to elute the product into HPLC loading vial, pre-filled with WFI (3.0 mL). The entire contents of vial are transferred into the HPLC injector loop for purification. Purification is performed by HPLC using a semi-preparative Chiralcel OJ-H column (5 µm, 250 x 10 mm) connected to a Phenomenex Luna C18 (2) (10 µm, 250 x10 mm) and eluted with a mixture of acetonitrile/ammonium acetate solution (5 mM) (40/60, v/v) at a flow rate of 4 mL/min. The product fraction is collected into the collection flask, containing 25 mL of ascorbic acid (10 mg/mL) in WFI. The diluted product mixture is passed through a tC18 solid-phase extraction cartridge and the cartridge is rinsed with 10 mL of ascorbic acid (10 mg/mL) in WFI. The radiolabeled product is eluted from the SPE cartridge with 1 mL of 200-proof USP grade ethanol into the formulation flask, pre-loaded with 10 mL of formulation base (ascorbic acid (0.7 mg/mL) in 0.9% saline). The cartridge is rinsed with 4 mL of formulation base and the rinse is mixed with the contents of the formulation flask. The resulting solution is passed through a sterilizing 0.2 µm membrane filter into a sterile, filter-vented vial (final product vial, FPV).

Supplemental TABLE 1

^{18}F -MNI-800 kinetic parameters of 2T model in pooled rhesus and cynomolgus macaques (n = 4, mean \pm standard deviation (cov)).

Region	K_1	k_2	k_3	k_4	K_1/k_2	k_3/k_4
Striatum	0.28 \pm 0.06 (21%)	0.11 \pm 0.04 (38%)	0.039 \pm 0.052 (133%)	0.069 \pm 0.050 (72%)	2.69 \pm 0.45 (17%)	0.39 \pm 0.36 (92%)
Caudate	0.25 \pm 0.05 (20%)	0.10 \pm 0.04 (40%)	0.041 \pm 0.054 (130%)	0.062 \pm 0.044 (70%)	2.52 \pm 0.53 (21%)	0.46 \pm 0.40 (88%)
Putamen	0.31 \pm 0.08 (24%)	0.11 \pm 0.04 (37%)	0.037 \pm 0.051 (137%)	0.076 \pm 0.055 (73%)	2.86 \pm 0.41 (14%)	0.33 \pm 0.32 (96%)
Nucleus accumbens	0.24 \pm 0.05 (19%)	0.11 \pm 0.03 (26%)	0.020 \pm 0.024 (119%)	0.050 \pm 0.036 (72%)	2.19 \pm 0.19 (9%)	0.33 \pm 0.18 (53%)
Globus pallidus	0.21 \pm 0.06 (27%)	0.10 \pm 0.05 (45%)	0.052 \pm 0.066 (127%)	0.084 \pm 0.072 (86%)	2.18 \pm 0.45 (20%)	0.39 \pm 0.38 (97%)
Thalamus	0.27 \pm 0.06 (21%)	0.21 \pm 0.15 (70%)	0.037 \pm 0.046 (125%)	0.081 \pm 0.048 (59%)	1.61 \pm 0.62 (39%)	0.35 \pm 0.30 (84%)
Frontal cortex	0.21 \pm 0.02 (8%)	0.12 \pm 0.00 (2%)	0.007 \pm 0.002 (27%)	0.025 \pm 0.001 (4%)	1.79 \pm 0.12 (7%)	0.27 \pm 0.08 (30%)
Cerebellum	0.29 \pm 0.04 (15%)	0.20 \pm 0.04 (19%)	0.025 \pm 0.019 (73%)	0.075 \pm 0.052 (69%)	1.45 \pm 0.07 (5%)	0.34 \pm 0.13 (39%)

Supplemental TABLE 2

^{18}F -MNI-968 kinetic parameters of 2T model in pooled rhesus and cynomolgus macaques (n = 3, mean \pm standard deviation (cov)).

Region	K_1	k_2	k_3	k_4	K_1/k_2	k_3/k_4
Striatum	0.30 \pm 0.07 (23%)	0.21 \pm 0.22 (104%)	0.325 \pm 0.535 (165%)	0.111 \pm 0.095 (86%)	2.48 \pm 1.43 (58%)	1.55 \pm 2.24 (145%)
Caudate	0.26 \pm 0.04 (17%)	0.15 \pm 0.13 (84%)	0.206 \pm 0.322 (157%)	0.103 \pm 0.071 (70%)	2.36 \pm 1.24 (53%)	1.25 \pm 1.63 (131%)
Putamen	0.34 \pm 0.10 (28%)	0.26 \pm 0.30 (116%)	0.444 \pm 0.747 (168%)	0.118 \pm 0.120 (101%)	2.59 \pm 1.64 (63%)	1.84 \pm 2.86 (155%)
Nucleus accumbens	0.28 \pm 0.12 (42%)	0.20 \pm 0.19 (95%)	0.162 \pm 0.254 (156%)	0.094 \pm 0.080 (86%)	1.88 \pm 0.78 (42%)	1.04 \pm 1.22 (118%)
Globus pallidus	0.22 \pm 0.09 (41%)	0.13 \pm 0.12 (89%)	0.309 \pm 0.528 (171%)	0.159 \pm 0.214 (135%)	2.12 \pm 0.82 (39%)	0.83 \pm 1.25 (150%)
Thalamus	0.26 \pm 0.05 (21%)	0.18 \pm 0.12 (68%)	0.168 \pm 0.274 (163%)	0.124 \pm 0.120 (97%)	1.77 \pm 0.68 (39%)	0.72 \pm 0.97 (134%)
Frontal cortex	0.25 \pm 0.05 (18%)	0.13 \pm 0.02 (17%)	0.013 \pm 0.008 (58%)	0.041 \pm 0.027 (64%)	1.93 \pm 0.07 (4%)	0.33 \pm 0.03 (8%)
Cerebellum	0.30 \pm 0.08 (25%)	0.20 \pm 0.07 (33%)	0.332 \pm 0.487 (147%)	0.125 \pm 0.083 (66%)	1.53 \pm 0.14 (9%)	0.28 \pm 0.18 (64%)

Supplemental TABLE 3

^{18}F -MNI-800 (n=2) and ^{18}F -MNI-968 (n=1) V_T and BP_{ND} test-retest variability. ^{18}F -MNI-800 (^{18}F -MNI-968).

Region	V_T		BP_{ND}			
	2T	LGA	2T	LGA	SRTM	NI-LGA
Striatum	1.4% (7.5%)	3.3% (8.5%)	1.7% (16.2%)	3.6% (16.4%)	3.9% (14.8%)	3.7% (14.7%)
Caudate	1.9% (4.9%)	3.4% (6.2%)	3.2% (12.5%)	3.9% (13.1%)	4.3% (11.1%)	4.1% (11.1%)
Putamen	0.9% (9.7%)	3.3% (10.5%)	2.5% (18.9%)	3.4% (18.7%)	3.7% (17.5%)	3.5% (17.3%)
Nucleus accumbens	6.2% (0.7%)	2.2% (1.2%)	23.2% (1.9%)	11.1% (4.0%)	11.0% (0.0%)	11.2% (0.3%)
Globus pallidus	4.2% (1.4%)	3.8% (3.5%)	6.4% (7.2%)	6.8% (10.2%)	7.4% (9.8%)	6.9% (9.1%)
Thalamus	1.5% (9.1%)	2.0% (7.6%)	8.3% (37.9%)	6.9% (37.5%)	7.1% (41.2%)	6.8% (39.1%)
Frontal cortex	8.2% (4.3%)	3.1% (1.3%)	43.0% (11.5%)	24.7% (4.3%)	24.5% (15.1%)	24.9% (11.6%)
Cerebellum	2.1% (1.5%)	3.5% (0.4%)				

Supplemental TABLE 4

¹⁸F-MNI-800 (n=2) and ¹⁸F-MNI-968 (n=1) test-retest variability of kinetic parameters of 2T model. ¹⁸F-MNI-800 (¹⁸F-MNI-968).

Region	K₁	k₂	k₃	k₄	K₁/k₂	k₃/k₄
Striatum	7.2% (12.7%)	10.0% (9.5%)	83.0% (80.1%)	75.3% (67.0%)	5.2% (3.1%)	22.7% (13.4%)
Caudate	7.1% (11.4%)	11.5% (4.7%)	80.1% (46.1%)	61.8% (51.8%)	5.4% (6.7%)	23.0% (6.1%)
Putamen	7.1% (13.6%)	11.1% (13.4%)	87.2% (105.6%)	87.5% (78.2%)	5.2% (0.1%)	25.5% (34.5%)
Nucleus accumbens	5.4% (9.8%)	9.4% (4.3%)	77.9% (9.2%)	89.8% (35.7%)	4.7% (5.6%)	48.2% (26.8%)
Globus pallidus	8.3% (14.3%)	21.8% (25.9%)	126.8% (157.5%)	80.1% (122.2%)	13.6% (11.6%)	66.5% (68.0%)
Thalamus	11.0% (2.6%)	55.3% (7.2%)	166.0% (38.3%)	128.6% (69.8%)	46.4% (4.7%)	111.4% (101.3%)
Frontal cortex	6.2% (6.0%)	10.1% (10.3%)	15.5% (3.3%)	60.4% (40.2%)	5.0% (4.3%)	46.6% (36.9%)
Cerebellum	11.6% (20.4%)	13.1% (48.0%)	115.6% (154.1%)	104.9% (101.6%)	3.8% (28.3%)	19.4% (86.3%)

Supplemental TABLE 5

^{18}F -MNI-800 radiation absorbed dose estimates from whole body PET studies in 1 male and 1 female adult rhesus monkeys. The whole-body effective doses (ED) were estimated using the tissue weighting factors from ICRP-60.

	Dose (mSv/MBq)	
	Female	Male
Adrenals	1.58E-02	1.37E-02
Brain	8.05E-03	5.64E-03
Breasts	8.36E-03	NA
Gallbladder Wall	1.17E-01	7.88E-02
LLI Wall	2.21E-02	1.82E-02
Small Intestine	3.95E-02	3.16E-02
Stomach Wall	1.81E-02	1.12E-02
ULI Wall	4.31E-02	3.50E-02
Heart Wall	2.44E-02	1.92E-02
Kidneys	2.43E-02	2.89E-02
Liver	6.69E-02	6.38E-02
Lungs	1.83E-02	1.64E-02
Muscle	1.05E-02	8.54E-03
Ovaries	1.80E-02	NA
Pancreas	1.64E-02	1.36E-02
Red Marrow	1.22E-02	1.19E-02
Osteogenic Cells	1.61E-02	1.28E-02
Skin	7.31E-03	5.85E-03
Spleen	1.00E-02	1.09E-02
Testes	NA	1.05E-02
Thymus	1.05E-02	8.17E-03
Thyroid	8.00E-03	6.59E-03
Urinary Bladder Wall	1.46E-01	1.26E-01
Uterus	2.03E-02	NA
Total Body	1.27E-02	1.06E-02
ED (ICRP-60)	2.47E-02	2.11E-02